Check for updates

A novel nano-lanthanum complex: synthesis, characterization and application as a macrofuran chemosensor in pharmaceutical, biological and environmental samples†

Sheta M. Sheta, [ID] *[a] Mohkles M. Abd-Elzaher[a] and Said M. El-Sheikh [ID] [b]

Macrofuran is widely used as an antibiotic for the treatment of urinary tract infections. Nevertheless, it is prohibited due to toxicity and environmental concerns. The development of a fast, simple, and cost-effective approach for the determination of macrofuran antibiotic (MFA) is still a challenge. Herein, we report a chemosensor based on a nano-lanthanum complex derived from phenylenediamine. The physicochemical properties and structure of the prepared complex were confirmed using different spectroscopic tools such as X-ray diffraction (XRD), scanning electron microscopy equipped with EDX, elemental analysis, Fourier transform-infrared (FT-IR) spectroscopy, UV-vis spectroscopy, mass spectroscopy and photoluminescence (PL). The nano-lanthanum complex was found to be chemically stable, highly sensitive and selective to MFA, without interference from other common antibiotics. The limit of detection for MFA was 0.025 ng mL^{-1}, over a linear concentration range of 0.02–30.0 ng mL^{-1}, with a correlation coefficient of 0.994. The nano-lanthanum complex can be used successfully as a promising chemosensor for MFA determination in pharmaceutical formulation and different biological samples (whole blood–serum–plasma). In addition, this approach will protect human beings from the environmental hazards of antibiotics through the detection of the low limit of MFA. Meanwhile, the mechanism of interaction between the nano-lanthanum complex and MFA was studied and investigated.

Introduction

Macrofuran (MFA), a trade name for nitrofurantoin (NFT) antibiotic, is the most commonly used antibiotic in our country. The chemical structure is shown in Fig. S1.† It is a synthetic antimicrobial broad-spectrum antibiotic (nitrofuran family), used for treating the cases of urinary tract infections due to its sensitivity toward various Gram (+/−) bacteria (strains of *E. coli*, *Enterococci*, *S. aureus* and certain species of *Klebsiella*, *Enterobacter* and *Proteus* bacteria).[1,2] It is used not only locally, but also worldwide for humans and animals. For example, it is used as a treatment for antibacterial and anti-protozoan infections, and preventing their growth promotion in the additive feed for aquaculture and livestock.[3,4]

Unfortunately, some of the metabolites of the nitrofuran family antibiotics exhibit potential teratogenicity, cytotoxicity and environmental hazards. In addition, some of these antibiotics have a lot of side effects on pregnant women and cause some hepatic issues after short/long treatment courses.[1] Therefore, the European Union (EU), USA and few other countries have prohibited the use and administration of any nitrofuran products like furazolidone in 1995 (ref. 3 and [5]).

Due to the broad applications of NFT antibiotics as well as their vital disadvantages, many research studies desired for NFT and metabolization. Moreover, a large number of researchers are interested in the innovation and development of fast, simple, specific and sensitive analytical techniques and approaches for the detection of traces of these types of antibiotics. There are many analytical techniques for NFT detection such as electrochemical sensors,[1,3,6] voltammetric method,[5] spectrofluorimetric method,[7,8] flow injection-spectrophotometry,[9] chemiluminescence approach,[10] surface enhanced Raman spectroscopy,[11] and UHPLC-DAD assay.[12] Nevertheless, most of the reported methods have many advantages and limitations.

On the other hand, the metal complexes especially at the nanoscale and nanomaterials generally have a lot of properties and advantages.[13–18] They have a relatively large surface area with respect to particle size.[19] In addition, numerous nanomaterials are highly magnetic, semi-conductive, excellent adsorbent materials, and have promising physicochemical properties. These make the nanomaterials very selective and

[a]*Inorganic Chemistry Department, National Research Centre, 33, El-Behouth St., Dokki, Giza, 12622, Egypt. E-mail: dr.sheta.nrc@gmail.com; Fax: +20-02-33370931; Tel: +20 1009697356*

[b]*Nanomaterials and Nanotechnology Department, Central Metallurgical R & D Institute, Cairo, 11421, Egypt*

† Electronic supplementary information (ESI) available. See DOI: 10.1039/d0ra10116h

sensitive tools for the detection of organic molecules and can be easily interacted with a biological target more efficiently than bulk materials.[20] Lanthanum complexes and MOFs vital examples for metal complexes, incubated in a considerable analytical application. For example, it is used for the detection of ascorbic acid in pharmaceutical preparations,[21] as chemosensors for nitrofurans,[22] iron(III),[23] and for anthelmintic drugs.[24]

In the present work, a novel nano-lanthanum complex was prepared *via* a simple reaction of lanthanum chloride with 1,2-phenylenediamine. The complex produced was characterized using many analytical techniques and then used as a chemosensor for pharmaceutical, biological and environmental applications. The results revealed that the photoluminescence (PL) emission spectrum of the nano-lanthanum complex was adeptly enhanced as the concentration of macrofuran antibiotic (MFA) increased. Therefore, the nano-lanthanum complex could be used profitably as a promising chemosensor for the determination of MFA concentration. No interference from some biological molecules and commonly administered drugs and even nitro-antibiotics with similar structures to MFA was observed. Additionally, a comparison between the previously published works with the present approach is performed. The comparison revealed that the detection of MFA based on the nano-lanthanum complex is faster, simpler, inexpensive, highly sensitive, more selective, portable, and has a wide linear range and lower detection limit than previous reports (at 0.025 ng mL^{-1} to 0.10 nM MFA) and is easier to operate. Additionally, the present approach is applicable in different real samples such as biological samples (serum, plasma and urine samples) and pharmaceutical formulation. The analytical and statistical reproducibility, repeatability, accuracy and precision of the developed chemosensor are investigated as well as the mechanism of enhancement. The chemical stability of the prepared nano-lanthanum complex was also investigated.

Results and discussion

Nano-lanthanum complex characterization

The nano-lanthanum complex was prepared *via* a simple reaction of lanthanum chloride with 1,2-phenylenediamine according to Scheme S1.† The obtained orange-red precipitate was filtered, washed and finally dried. The structure was elucidated based on the obtained analytical data and discussed as follows:

FE-SEM/EDX spectroscopy. The nano-lanthanum complex FE-SEM images and EDX results are shown in Fig. 1. The morphology based on FE-SEM images at different magnification (Fig. 1a–c) appeared to be uniform rods, as shown in Fig. 1a. However, Fig. 1b and c shows the external surface of the rods, which appeared similar to the rods of the palm tree. The external surface consists of nano-rods with an average size of 108 nm. Moreover, the EDX mapping analysis (Fig. 1d and Table S1†) of the nano-lanthanum complex shows the presence of lanthanum, carbon, nitrogen, and oxygen as elemental building blocks in each single particle. The good distribution of the above elements along the cross-section shown by EDX analysis (Fig. 1d) confirmed the nano-lanthanum complex structure
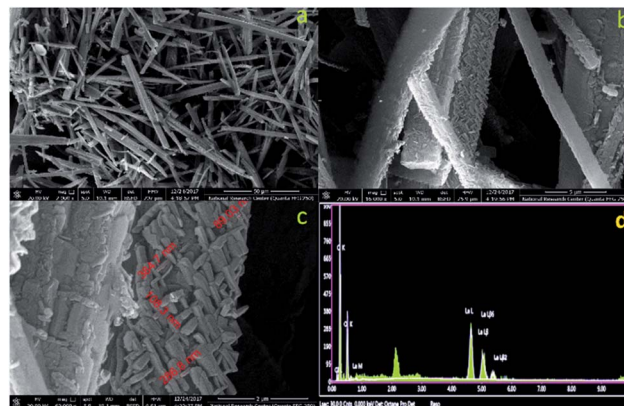

Fig. 1 (a–c) The field-emission scanning electron microscopy images at different magnification, (d) energy-dispersive X-ray analysis with a single point EDX mapping analysis of the nano-lanthanum complex.

formation. Furthermore, from Table S1† the stated EDX table results were in good conformity with that theoretically calculated: theoretically; C, 43.57; La, 22.90; N, 13.86; O, 13.19; found: C, 43.85; La, 22.91; N, 13.15; and O, 13.09.

Mass spectroscopy. The mass spectrum of the prepared nano-lanthanum complex and suggested scheme of fragmentation are presented in Fig. S2 and Scheme S3,† respectively. From Fig. S2,† it can be seen that the m/z peak completely agreed with the proposed empirical formula gained by elemental analysis. The theoretical molecular ion peak was calculated at 606.50 m/z. The subsequent mass fragmentations, as represented in Scheme S3,† were in good agreement with the suggested molecular structure $C_{22}H_{39}LaN_6O_5$. The ion of $m/z = 606.50$ underwent fragmentation to exhibit peaks at $m/z = 560$, 514, 496, 478, and 460 by losing two ethanol and three water molecules. Then, the further decomposition of the compound leads to the fragments with $m/z = 325, 138, 108, 107, 91, 80$, and 64. Generally, the successive fragmentation of the nano-lanthanum complex were in complete agreement with the theoretically calculated values and with the obtained molecular structure.[25]

FT-IR spectroscopy. The nano-lanthanum complex spectrum is shown in Fig. S3.† The peaks at 3400, 3310, 2973, and 1131 cm^{-1} are due to NH$_2$, O–H, C–H and C–O stretching of ethanol molecules.[26,27] The peak at 3210 cm^{-1} is assigned to the stretching of N–H. The sharp bands between 1525 and 1485 cm^{-1} are due to the stretching of C=C.[28,29] The bands between 1129 and 1055 cm^{-1} are attributed to C–H. The band at 584 cm^{-1} is assigned to a mixture of the covalent and ionic bonding of lanthanum ion with nitrogen ν(La–N).[30–33]

UV-vis spectroscopy. The electronic absorption spectrum of the nano-lanthanum complex is presented in Fig. S4.† From Fig. S4† it can be observed that the nano-lanthanum complex displays absorption bands at 266, 315, 397, 473, 588 and 642 nm. These bands can be attributed to intra-ligand π–π*, n–π*, and LMCT interactions.[30–33]

XRD analysis. The powder XRD spectrum of the nano-lanthanum complex is shown in Fig. S5.† The XRD spectrum

shows no sharp peaks, which indicates that the complex is almost amorphous. Moreover, the lattice parameters were in good agreement with JCPDS card no. 04-0856 of nanoparticles of lanthanum oxide. The observed peaks at 23°, 28°, and 32° correspond to the (*hkl*) values (101), (222), and (300), respectively. The details of the XRD data, lattice parameter values, Miller indices, interplanar distances and crystallite size of the nano-lanthanum complex were estimated *via* the Scherrer equation and are presented in Tables S2 and S3.† It can be noted from the table data that the crystallite size was between 71 and 113 nm (ref. 34).

Thermal analysis. The thermal behavior of nano-lanthanum complex (TGA/DTGA) plots (Fig. S6†) suggested that the nano-lanthanum complex underwent three breakdown stages. A weight loss of 24.1% was observed due to the loss of ethyl alcohol and water molecules in the temperature range of 59.84 to 122.0 °C (calculated weight loss: 24.03%). The nano-lanthanum complex followed a second decomposition stage with a weight loss of 53.71% due to the exclusion of organic phenyl rings between 306.0 and 385.0 °C. The remaining residue and last stage is (22.18%) due to La and La_2O_3. The obtained data was in agreement with that obtained from XRD data.

Based on the above discussed physical, analytical and spectral data, we can deduce the 3D structure of the nano-lanthanum complex and the advanced molecular surface as represented in Fig. 2a and b, respectively.

Chemical stability of the nano-lanthanum complex. The chemical stability of the nano-lanthanum complex was accomplished *via* investigating the thermogravimetric behavior of the complex in addition to other parameters, such as the solvents, temperature, and time effect. Herein, the FT-IR spectrum and P-XRD patterns of the nano-lanthanum complex (Fig. 3a and b, respectively) were investigated three times (initial analysis then after 2 and 4 months) at room temperature. From Fig. 3a and b, the FT-IR spectrum and P-XRD patterns were quite similar to those obtained for the original sample. This indicates that the lanthanum complex is stable chemically under storage conditions. Furthermore, the chemical stability of the nano-lanthanum complex in different solvents was evaluated, as shown in Fig. 3c. From Fig. 3c, it can be seen that there is an emission band at 573 nm after excitation at 365 nm in the PL spectrum of the nano-lanthanum complex in various solvents, which proves the stability of the lanthanum complex in various solvents. Finally, from the thermal behavior of the prepared
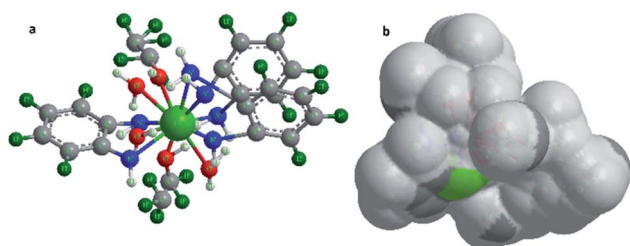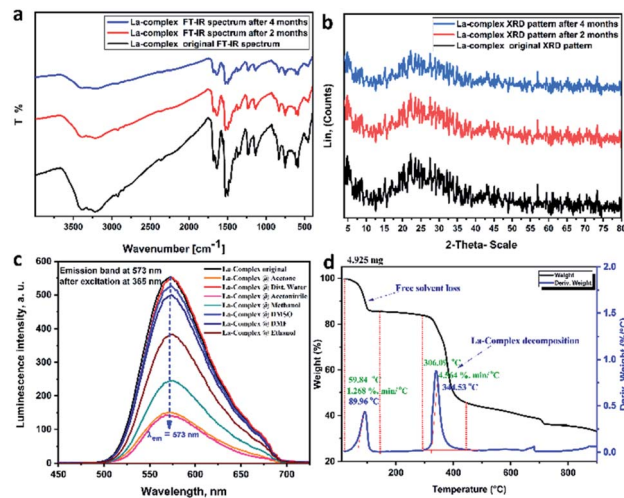

Fig. 3 The chemical stability study of the nano-lanthanum complex. (a) The FT-IR spectrum of nano-lanthanum complex after storing it in a fit test tube for 2 months and 4 months, (b) the XRD patterns of nano-lanthanum complex after storing it in a fit test tube for 2 months and 4 months, (c) the PL spectrum of nano-lanthanum complex after dissolving in different solvents and leaving for one day, and (d) the thermogravimetric analysis of the nano-lanthanum complex.

nano-lanthanum complex (Fig. 3d) it shows two stages of decomposition due to the loss of free solvent molecules at 89.96 °C and then the lanthanum complex starts to decompose at a temperature of 306.09 °C. The obtained results indicate the stability of the lanthanum complex at high temperature.

Photoluminescence (PL) studies and applications. The PL spectrum at different excitation wavelengths of the nano-

Fig. 2 (a) 3D structural representation, (b) advanced molecular surface representation of the nano-lanthanum complex.
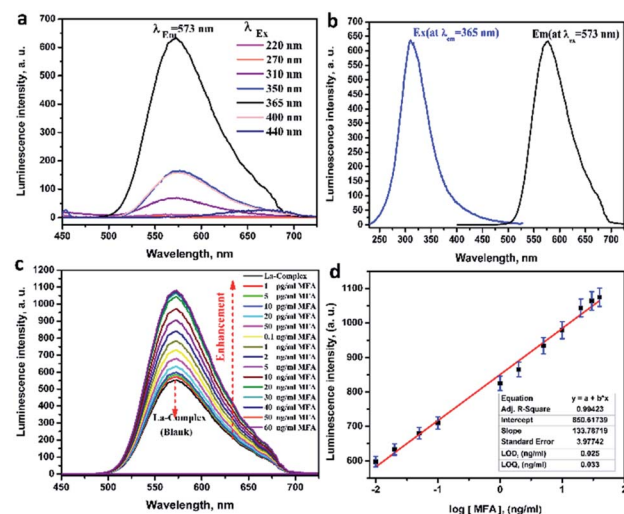

Fig. 4 (a) The photoluminescence emission spectrum at different excitation wavelength for the nano-lanthanum complex, (b) excitation (blue line) and emission (black line) spectra for the nano-lanthanum complex, (c) the photoluminescence emission spectra for investigating the behaviour of the nano-lanthanum complex towards different concentrations of MFA, (d) a linear relationship (calibration graph) between the photoluminescence intensity of the nano-lanthanum complex and the logarithm MFA concentration (log[MFA]).

lanthanum complex was recorded at RT as presented in Fig. 4a. From this figure, the nano-lanthanum complex exhibits an emission band at 573 nm after excitation at 365 nm under ideal conditions. The excitation and emission spectra are presented in Fig. 4b. The fluorescence behavior of the nano-lanthanum complex can be attributed to intra-ligand $\pi-\pi^*$ and $n-\pi^*$ interactions, and due to the molecular orbital transitions in the ligand–metal charge transfer (LMCT).

The nano-lanthanum complex was used as a spectro-fluorimetric chemosensor for MFA. The PL spectrum (at λ_{ex} = 365 nm) of the nano-lanthanum complex (10 mM) was investigated against different concentrations of MFA and the data is presented in Fig. 4c. As shown in Fig. 4c, the PL intensity spectrum of the nano-lanthanum complex was remarkably enhanced as the MFA concentration increased from 1 pg mL^{-1} to 60 ng mL^{-1}. These results prove that the nano-lanthanum complex could be considered as a spectrofluorimetric chemosensor for MFA detection.

Calibration curve, limit of detection and limit of quantification. The calibration curve (standard curve) between the PL intensity of nano-lanthanum complex at λ_{em} = 573 nm and the concentration of MFA in a range between 1.0 pg mL^{-1} and 60.0 ng mL^{-1} are presented in Fig. S7.† Under the optimum PL conditions, the linear dynamic graph for the nano-lanthanum PL chemosensor (Fig. 4d) was investigated. From Fig. 4d, the spectral PL was highly dependent on the concentration of MFA; the PL λ_{573} increased and saturates at a MFA concentration of 1.0 pg mL^{-1}.

The calibration plot shows a linear relationship over a range of 0.02–30.0 ng mL^{-1}. The fitting equations can be expressed as:

$$\text{Nano-lanthanum PL intensity} = 580.617 + 133.787 \log[\text{MFA}]$$
$$\text{with } r^2 = 0.994.$$

The LOD for the nano-lanthanum spectrofluorimetric chemosensor was found to be 0.025 ng mL^{-1}, whereas the LOQ was 0.033 ng mL^{-1}. A summary of the regression data analysis of PL is presented in Table S4.† From the above discussion and table data, the lower values of LOD and LOQ and wide linear range for the proposed chemosensor confirm its extreme sensitivity. Furthermore, the LOD and LOQ values are better and lower than the other previously published articles and the data are summarized in Table 1.
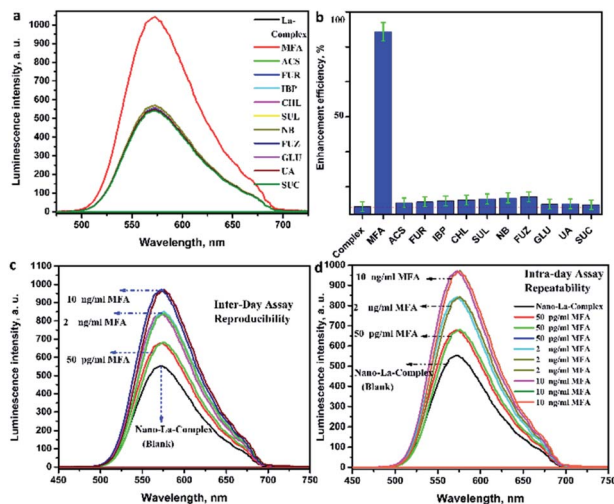
Selectivity. We next confirmed the specific detection ability of the nano-lanthanum complex towards MFA based on the suggested photoluminescence approach. The PL spectra of the nano-lanthanum complex (10 mM) were studied against different interfering analytes (acetylsalicylic acid (ACS), furosemide (FUR), ibuprofen (IBP) as examples for co-administered drugs; chloramphenicol (CHL), sulfafurazole (SUL), nitrobenzene (NB), furazolidone (FUZ) as examples for nitro-compounds with similar structure with MAF; glucose (GLU), uric acid (UA), sucrose (SUC) as biological molecules), at the analyte concentration 20 ng mL^{-1}. Each compound was tested out in a separate single test against the nano-lanthanum complex. The results of the PL study are presented in Fig. 5a and b, which shows the PL spectrum and the histogram of enhancement efficiency, respectively. From Fig. 5a and b, the nano-lanthanum complex exhibited a remarkably enhanced response with an observed increase in the PL intensity in the case of MFA. At the same time, it did not give any noticeable response to the other interfering analytes. Therefore, we can deduce that the nano-lanthanum complex is extremely selective and specific for MFA throughout the exceptional enhancement phenomenon.

Accuracy, precision, reducibility and repeatability. In this study, statistical evaluations for the applicability and effectiveness of the proposed methodology were performed based on the nano-lanthanum complex to quantify the MFA concentration. Three levels of MFA concentrations 50 pg mL^{-1}, 2 ng mL^{-1}, and 10 ng mL^{-1} were used and each reading was repeated three times per day (to check the repeatability) and on different days (to check the reproducibility). The PL spectra of the nano-lanthanum complex towards different concentrations of MFA

Table 1 Comparison between the nano-lanthanum complex chemosensor and some existing methods for the determination of MFA

Method	Linear detection range	LOD	Ref.
Electrochemical sensor based on lanthanum molybdate nanospheres	0.01–144.0 μM	72.00 nM	1
Electrochemical sensor based on reduced graphene oxide/Fe$_3$O$_4$	0.005–100.0 μM	1.14 nM	3
Voltammetric method	1.0–1000 nM	0.15 nM	5
Electrochemical sensor based on molecularly imprinted copolymer	0.001–0.05 μM; 0.100–1.0 μM	0.30 nM	6
Spectrofluorimetric method	0.085–1.01 μM	8.00 nM	7
Label-free photoluminescence assay	0.05–4.00 μM	30.00 nM	8
Flow injection-spectrophotometry	0.021–1.27 nM	8.03 nM; 20.28 nM	9
Electrogenerated chemiluminescence	10.0–100.0 μM	0.60 μM	10
Surface enhanced Raman spectroscopy	2.11–42.25 μM	0.211 μM	11
UHPLC-DAD assay	0.211–5.28 nM; 0.017–0.85 nM	0.114 nM; 0.19 nM	12
Nano-lanthanum complex chemosensor	0.02–30.0 ng mL^{-1} to (0.08–126.8 nM)	0.025 ng mL^{-1} to (0.10 nM)	The present work

Fig. 5 (a) The photoluminescence intensity of the nano-lanthanum complex toward the MFA against different types of interfering analytes, (b) the photoluminescence enhancement efficiency histogram of nano-lanthanum complex toward the MFA against different types of interfering analytes, (c) the photoluminescence intensity of the nano-lanthanum complex for evaluating the inter-day accuracy and precision, (d) the photoluminescence intensity of the nano-lanthanum complex for evaluating the intra-day accuracy and precision. [Macrofurans (MFA), acetylsalicylic acid (ACS), furosemide (FUR), ibuprofen (IBP), chloramphenicol (CHL), sulfafurazole (SUL), nitrobenzene (NB), furazolidone (FUZ), glucose (GLU), uric acid (UA), sucrose (SUC)].

are shown in Fig. 5c and d, respectively. In addition, the summarized results are presented in Table S5.†

The analysis of the output table data shows that the calculated relative error percent (RE%) values were between 1.0 and 1.003%; intra-day; and 0.943 and 1.004%; inter-day, which implies excessive accuracy, repeatability and reducibility of the

proposed methodology. Moreover, the evaluated values of mean (X) were in target, the standard deviation (SD) were between 1.77 and 2.16%; intra-day; and 1.54 and 3.14%; inter-day, the coefficient of variation (CV) values are between 0.003 and 3.12%; intra-day; and 1.16 and 4.07%; inter-day. The extra-low values of SD as well CV imply the excellent precision, reducibility and repeatability of suggested methodology.

Analytical applications in real samples and recovery study. The currently proposed methodology was investigated to quantify the MFA concentration content in several types of real samples; biological samples (serum, plasma and urine samples) and in pharmaceutical formulation. The MFA standard was spiked in biological samples at three levels of concentrations 10.0 pg mL^{-1}, 1.0 ng mL^{-1} and 30.0 ng mL; each test was repeated three times. The pharmaceutical formulation (macrofuran capsules, 100 mg) was tested at the same concentration levels. The obtained results are presented in Tables 2 and 3.

The statistical evaluations for pharmaceutical formulation samples were carried out by the calculation of the percent recoveries (RC%) and relative standard deviation (RSD%). These data demonstrate that the average RC ± RSD% are 100.4 ± 2.66% for serum samples, 95.3 ± 3.01% for plasma samples, 101.4 ± 1.75% for urine samples, 95.44 ± 2.25%. The data obtained above demonstrate that the proposed methodology is applicable and effective for the quantification of MFA in different biological samples and pharmaceutical formulation. Moreover, this approach will be a potential critical analytical tool in the future, which will help, address and monitor a vital environmental issue and human health issue related to MFA quantification.

The mechanism of fluorescence. The fluorescence enhancement mechanism of the sensing platform (nano-

Table 2 Determination of MFA in different real samples using nano-lanthanum complex chemosensor

Sample	Spiked MFA^a (ng mL^{-1})	Found^a (ng mL^{-1})	RSD%	Recovery%
Serum	0.01	0.01	3.25	100.00
	1.00	0.999	1.47	99.90
	30.00	30.40	3.25	101.30
Plasma	0.01	0.009	3.57	90.00
	1.00	0.972	2.57	97.20
	30.00	29.63	2.89	98.77
Urine	0.01	0.011	2.12	105.00
	1.00	0.97	0.998	97.30
	30.00	30.56	2.14	101.90

^{a} Each reading was repeated three times; RSD, relative standard deviation.

Table 3 Determination of MFA in pharmaceutical formulation using nano-lanthanum complex chemosensor

Sample	Concentration of MFA^a (ng mL^{-1})	Found^a (ng mL^{-1})	RSD%	Recovery%
Pharmaceutical formulation	0.01	0.0089	3.47	89.00
	1.00	0.982	2.14	98.20
	30.00	29.74	1.15	99.13

^{a} Each reading was repeated three times; RSD, relative standard deviation.

lanthanum complex) can be investigated as follows: as represented in Fig. 4c, it can be seen that with an increase in the MFA concentration the emission intensity of the nano-lanthanum complex increases, and this is evidence of an interaction between the nano-lanthanum complex and MFA. The noted sensing platform behaviour of the nano-lanthanum complex towards MFA may be ascribed to intra-ligand π–π^* and n–π^* interactions, and due to the molecular orbital transitions in the ligand–metal charge transfer (LMCT).[18,35,36] Moreover, the lipophilic properties of the nano-lanthanum complex are enhanced due to the delocalization of π electrons in the aromatic ring, and according to the chelation theory, the polarity of the metal ion decreases.[37,38] In addition, due to the decrease in the polarity, the probability of chelating with the ligand (MFA) is increased and the interactions of the nano-lanthanum complex with MFA are normally due to covalent and ionic bonding.[37–39]

Experimental

Materials & instruments

See the (ESI file†) for details.

Procedure

Synthesis of the nano-lanthanum complex. The nano-lanthanum complex was prepared according to Scheme S1† *via* a reaction of lanthanum chloride (1.0 mmol, 0.3714 g) in 10 mL distilled water with 1,2-phenylenediamine (3.0 mmol, 0.3245 g) dissolved in 10 mL ethanol; the system was stirred at room temperature (RT) for 24 hours. An orange-red precipitate was obtained. This precipitate was filtered, washed, and dried. The elemental analysis of the prepared nano-lanthanum complex was in great conformity with the theoretically calculated chemical formula; anal. calc. (%): $C_{22}H_{39}LaN_6O_5$, (606.50 g mol^{-1}), C, 43.57; H, 6.48; N, 13.86; found C, 43.14; H, 6.46; N, 13.15; and the yield was 47.5%.

General procedure for PL measurement. The photoluminescence (PL) measurements were performed with a spectro-fluorophotometer instrument at RT in a quartz cuvette with 1 cm path length, and scan time of 30 s according to Scheme S2.† The prepared samples for the present study were used for subsequent PL measurements. First, at RT, 1 mM stock solution of the nano-lanthanum complex was prepared by dissolving a suitable weight in DMF. The working solution (10 mM) was afforded from the stock solution by dilution with distilled water. The nano-lanthanum complex solution (10 mM) was exhausted for consequent PL measurements at different excitation wavelengths for select the optimal excitation wavelength upon the maximum emission wavelength. Second, upon the optimization of the PL measurement conditions and selection of the λ_{em} and λ_{ex}, the nano-lanthanum complex was used for the determination of MFA according to the protocol in the following section. Third, a statistical study of the analytical performance of the current chemosensor and comparison with other published methods for MFA determination was performed.

Determination of MFA using the nano-lanthanum complex and application in real samples. The PL spectrum of the nano-lanthanum complex (10 mM) against freshly prepared MFA at different concentrations was investigated. Upon the optimization of the PL measurement conditions, a linear relationship was found between the PL intensity of the nano-lanthanum complex at $\lambda_{em} = 573$ nm after $\lambda_{ex} = 365$ nm, in the concentration range between 0.02 and 30 ng mL^{-1} MFA. According to the least-squares method, the equation parameters and correlation coefficient (r^2) were calculated. The regression equation was: $Y = a + bX$ where Y is the PL intensity of the nano-lanthanum complex at $\lambda_{em} = 573$ nm; a is the intercept; b is the slope; and X is the MFA concentration. Furthermore, the limit of detection (LOD) and the limit of quantification (LOQ) were computed by the equations: LOD = $3.3(S/b)$ & LOQ = $10(S/b)$[40,41] where S is the standard error value of PL intensity; b is the slope of the relationship graph. The PL spectrum of the nano-lanthanum complex was also investigated against different interfering analytes and against different real samples spiked with different concentrations of MFA.

The pharmaceutical formulation (macrofuran capsules, 100 mg) *i.e.* five capsules from macrofuran were opened and carefully weighed under an inert atmosphere. A precise equivalent weight to 100 mg of macrofuran was transferred to a 50 mL beaker and dissolved efficiently in distilled water. Then, the solution was filtered and transferred to a volumetric flask (100 mL). The flask was filled to the mark with distilled water to obtain the stock solution from which the working solutions were prepared.

Conclusions

This work presents a spectrofluorimetric approach based on a novel promising nano-lanthanum complex, which was prepared and well characterized. The morphology of the prepared complex appeared to be uniform rods like those of the palm tree with an external surface consisting of nano-rods with an average size of 108 nm. Moreover, the chemical stability results showed significant stability of the nano-lanthanum complex. Therefore, the nano-lanthanum complex could be used profitably as a promising chemosensor for the determination of MFA concentration in pharmaceutical formulation and different biological samples (serum, plasma, and whole blood). The statistical evaluation of the proposed approach, in general, was fit for the purpose. The LOD for MFA was 0.025 ng mL^{-1}, over a linear concentration range 0.02–30.0 ng mL^{-1}, with r^2 of 0.994. Comparison of the current work with the other published reports revealed this approach to be fast, simple, inexpensive, more sensitive, extremely selective, not time-consuming, with lower LOQ/LOD, wider dynamic linear ranges and applicability for different types of biological samples and pharmaceutical formulation. The results revealed a promising crucial tool for monitoring and quantification of MFA, which is a vital environmental and public human health issue.

Conflicts of interest

There are no conflicts to declare.

Acknowledgements

Notes and references

1 B. Karuppaiah, R. Ramachandran, S.-M. Chen, S. Wan-Ling and J. Y. Wan, *New J. Chem.*, 2020, **44**, 46–54.
2 R. Gleckman, S. Alvarez and D. W. Joubert, *Am. J. Hosp. Pharm.*, 1979, **36**, 342–351.
3 B. He and J. Li, *Anal. Methods*, 2019, **11**, 1427–1435.
4 M. Vass, K. Hruska and M. Franek, *Vet. Med. (Praha).*, 2008, **53**, 469–500.
5 D. Dechtrirat, P. Yingyuad, P. Prajongtat, L. Chuenchom, C. Sriprachuabwong, A. Tuantranont and M. Tang, *Microchim. Acta*, 2018, **185**, 261–270.
6 M. Roushani and Z. Rahmati, *J. Iran. Chem. Soc.*, 2019, **16**, 999–1006.
7 T. S. Belal, *J. Fluoresc.*, 2008, **18**, 771–780.
8 Y. Wang, T. Chen, Q. Zhuang and Y. Ni, *Talanta*, 2018, **179**, 409–413.
9 H. Hadi and M. Mouayed, *J. Assoc. Arab Univ. Basic Appl. Sci.*, 2017, **24**, 74–80.
10 N. Taokaenchan, T. Tangkuaram, P. Pookmanee, S. Phaisansuthichol, S. Kuimalee and S. Satienperakul, *Biosens. Bioelectron.*, 2015, **66**, 231–237.
11 Y. Zhang, Z. Yu, Z. Yue, J. Gao, S. Wu, Z. Zhang and G. Li, *J. Raman Spectrosc.*, 2019, **50**, 1094–1102.
12 R. A. Wijma, K. E. J. Hoogtanders, S. Croes, J. W. Mouton and R. J. M. Brüggemann, *J. Pharm. Biomed. Anal.*, 2019, **174**, 161–167.
13 S. M. Sheta, S. M. El-Sheikh and M. M. Abd-Elzaher, *Appl. Organomet. Chem.*, 2019, **33**, e5069.
14 S. M. Sheta, S. M. El-Sheikh, M. M. Abd-Elzaher, S. R. Salem, H. A. Moussa, R. M. Mohamed and I. A. Mkhalid, *Appl. Organomet. Chem.*, 2019, **33**, e5249.
15 S. Liu, L. Wang, J. Tian, Y. Luo, G. Chang and A. M. Asiri, *Chempluschem*, 2012, **77**, 23–26.
16 L. H. Abdel-Rahman, A. M. Abu-Dief, R. M. El-Khatib and S. M. Abdel-Fatah, *Bioorg. Chem.*, 2016, **69**, 140–152.
17 M. A. Akl, E. R. El-gharkawy, N. A. El-mahdy, S. M. El-sheikh and S. M. Sheta, *Dalton Trans.*, 2020, **49**, 15769–15778.
18 M. Alhaddad and S. M. Sheta, *ACS Omega*, 2020, **5**, 28296–28304.
19 S. M. Sheta, S. M. El-Sheikh and M. M. Abd-Elzaher, *Dalton Trans.*, 2018, **47**, 4847–4855.
20 S. M. Sheta, M. A. Akl, E. Saad and E. R. H. El-gharkawy, *RSC Adv.*, 2020, **10**, 5853–5863.
21 F. A. O. Olgun, D. Ozyurt, K. I. Berker, B. Demirata and R. Apak, *J. Sci. Food Agric.*, 2014, **94**, 2401–2408.
22 F. Zhang, H. Yao, T. Chu, G. Zhang, Y. Wang and Y. Yang, *Chem.–Eur. J.*, 2017, **23**, 10293–10300.
23 S. M. Sheta, S. M. El, S. Mohkles, M. A. Elzaher and A. R. Wassel, *Appl. Organomet. Chem.*, 2019, **33**, e4777.
24 S. M. Derayea, A. A. Hamad, D. M. Nagy, D. A. Nour-eldeen, H. Refat, H. Ali and R. Ali, *J. Mol. Liq.*, 2018, **272**, 337–343.
25 K. Henrick, D. L. Kepert, E. Shewchuk, K. R. Trigwell and S. B. Wild, *Aust. J. Chem.*, 1974, **27**, 727–739.
26 S. M. Sheta, S. M. El-sheikh, D. I. Osman, A. M. Salem, O. I. Ali, F. A. Harraz, W. G. Shousha, M. A. Shoeib, S. M. Shawky and D. D. Dionysiou, *Dalton Trans.*, 2020, **49**, 8918–8926.
27 A. S. Basaleh and S. M. Sheta, *Anal. Bioanal. Chem.*, 2020, **412**, 3153–3165.
28 B. M. Omkaramurthy and G. Krishnamurthy, *Inorg. Nano-Met. Chem.*, 2019, **49**, 375–384.
29 D. K. Yadav, R. Gupta, V. Ganesan, P. K. Sonkar and M. Yadav, *ChemElectroChem*, 2018, **5**, 2612–2619.
30 A. I. Othman, I. R. Kaiss and A. H. Huda, *Res. J. Chem. Environ.*, 2019, **23**, 43–49.
31 A. S. Shawali, S. Elsheikh and C. Párkányi, *J. Heterocycl. Chem.*, 2003, **40**, 207–212.
32 A. S. Shawali, A. A. Elghandour and S. M. El-sheikh, *J. Prakt. Chem.*, 2000, **342**, 96–99.
33 S. M. El-shiekh, M. M. Abd-Elzaher and M. Eweis, *Appl. Organomet. Chem.*, 2006, **20**, 505–511.
34 K. Bikshalu, V. S. K. Reddy, P. C. S. Reddy and K. V. Rao, *Int. J. Adv. Syst. Soc. Eng. Res.*, 2014, **4**, 12–15.
35 S. M. Sheta, S. M. El-sheikh and M. M. Abd-elzaher, *Anal. Bioanal. Chem.*, 2019, **411**, 1339–1349.
36 A. S. Basaleh and S. M. Sheta, *J. Inorg. Organomet. Polym. Mater.*, 2021, DOI: 10.1007/s10904-021-01888-4.
37 Y. Wu, W. Wu, L. Zou, J. Feng, C. Gu, B. Li, S. R. Batten, R. Yadav and A. Kumar, *Inorg. Chem. Commun.*, 2016, **70**, 160–163.
38 S. Pal, A. Bhunia, P. P. Jana, S. Dey, J. Möllmer, C. Janiak and H. P. Nayek, *Chem.–Eur. J.*, 2015, **21**, 2789–2792.
39 Y. Ito, K. Matsuda and Y. Kanemitsu, *Phys. Rev. B: Condens. Matter Mater. Phys.*, 2007, **75**, 033309.
40 M. M. Abd-Elzaher, M. A. Ahmed, A. B. Farag, M. S. Attia, A. O. Youssef and S. M. Sheta, *Sens. Lett.*, 2017, **15**, 977–981.
41 M. M. Abd-Elzaher, M. A. Ahmed, A. B. Farag, M. S. Attia, A. O. Youssef and S. M. Sheta, *Sens. Lett.*, 2017, **15**, 525–530.